JACS
JOURNAL OF THE AMERICAN CHEMICAL SOCIETY
pubs.acs.org/JACS

Article

A Broad-Spectrum Catalyst for Aliphatic Polymer Breakdown

Jiaxin Gao, Frédéric A. Perras, and Matthew P. Conley*

Cite This: J. Am. Chem. Soc. 2025, 147, 18145−18154

Read Online

ACCESS | Metrics & More | Article Recommendations | Supporting Information

ABSTRACT: Thermolysis of the well-defined aluminum fluoroalkoxide supported on silica (≡SiOAl(OC(CF$_3$)$_3$)$_2$(O(Si≡)$_2$), **1**, 0.20 mmol$_{Al}$ g^{-1}) at 200 °C forms a fluorinated amorphous silica−alumina (F-ASA) containing a distribution of Al(IV), Al(V), and Al(VI) sites that maintain relatively strong Lewis acidity. Small amounts of Brønsted sites are also present in F-ASA. Solid-state NMR studies show that a majority of the aluminum centers in F-ASA are not close to the Si−F groups that form during thermolysis. F-ASA is exceptionally reactive in cracking (or pyrolysis) reactions of neat polymer melts. Catalyst loadings as low as 2 wt % (0.017 mol % aluminum) efficiently break down isotactic polypropylene, high-density polyethylene, ethylene/1-octene copolymer, and postconsumer wastes. The major products of this reaction are hyperbranched liquid paraffins containing internal olefins and very small amounts of aromatics. Under continuous distillation of oils from the reaction mixtures, pyrolysis on 50 g reaction scales is feasible. F-ASA cokes and deactivates during this reaction but can be reactivated by calcination in air. These properties are complementary to other state-of-the-art catalysts for polymer breakdown, but unlike those catalysts F-ASA does not require an additional cofed reactant (e.g., H$_2$, olefin, etc.) to drive the reaction.

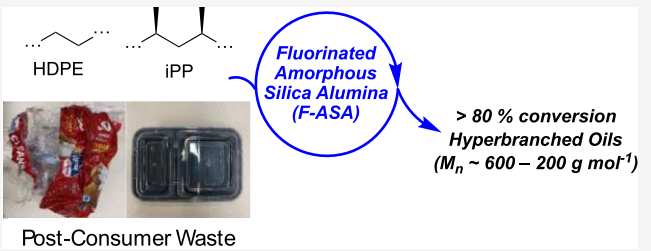

INTRODUCTION

Enormous amounts of plastic are produced each year. A vast majority of plastic materials reach end-of-life at an incinerator or in a landfill, the latter resulting in considerable leakage into the environment.[1] The small amounts of plastic that are recycled undergo mechanical processing that can result in poor material performance.[2] Chemical processes involving a catalyst or mixtures of catalysts that activate inert C−H and C−C bonds in polymers to form lower molecular weight products are emerging.[3]

Plastic waste streams contain vast amounts of polyethylene (PE) and isotactic polypropylene (iPP), ubiquitous hydrocarbon polymers in modern society. These materials should be compatible with catalysts used for thermal cracking reactions throughout the petrochemical industry, such as silica−alumina or zeolites,[4] to convert them into a broad portfolio of valuable small molecules.[5] This reaction would also provide a powerful method to deconstruct polymers because these catalysts are scalable and do not require additional chemical inputs (e.g., H$_2$, olefin, etc.) to initiate polymer breakdown. Silica−alumina or zeolite mediated cracking (or pyrolysis) of polymers usually result in modest product yields[3,6] with limited selectivity profiles.[7]

Amorphous silica−alumina (ASA) behaves similarly in polymer cracking reactions.[8] ASA is prepared by a variety of methods,[9] including deposition of a reactive alkoxide onto SiO$_2$ or Al$_2$O$_3$ followed by high-temperature calcination under air, Figure 1a.[9,10] This results in a complex network of SiO$_4$ tetrahedral framework elements and a distribution of four-, five-, and six-coordinate AlO$_x$ sites, some of which coordinate to silanols to form Brønsted sites of varying acidities.[11] How this distribution of sites affects polymer cracking reactions is not known.

Thermolysis of the well-defined aluminum fluoroalkoxide supported on silica (**1**),[12] shown in Figure 1b, forms fluorinated ASA (F-ASA). During thermolysis, an etching process also occurs, which replaces framework Si−O−Si linkages with Si−F groups (major) or opening of these linkages to form Si−OC(CF$_3$)$_3$ groups (minor). F-ASA catalyzes cracking reactions of PE, iPP, or ethylene/1-octene copolymer melts using catalyst loadings as low as 6000 monomer units per aluminum (0.017 mol % Al). F-ASA also cracks postconsumer waste and is tolerant of PVC in the reaction feed. The spent catalyst can be recycled by calcination under air. These properties are superior to available ASA materials in polymer degradation reactions.

EXPERIMENTAL SECTION

General Considerations. All reactions and manipulations were performed under an inert atmosphere of N$_2$ or Ar using glovebox or Schlenk techniques. **1** was previously reported.[12b] Briefly, solution of Al(OC(CF$_3$)$_3$)$_3$(PhF)[37b] in PhF was contacted with Aerosil-200 SiO$_2$ partially dehydroxylated at 700 °C (SiO$_{2-700}$, 200 m^2 g^{-1}, 0.26

Received: March 15, 2025
Revised: April 17, 2025
Accepted: May 1, 2025
Published: May 13, 2025

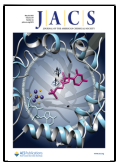

https://doi.org/10.1021/jacs.5c04524
J. Am. Chem. Soc. 2025, 147, 18145−18154

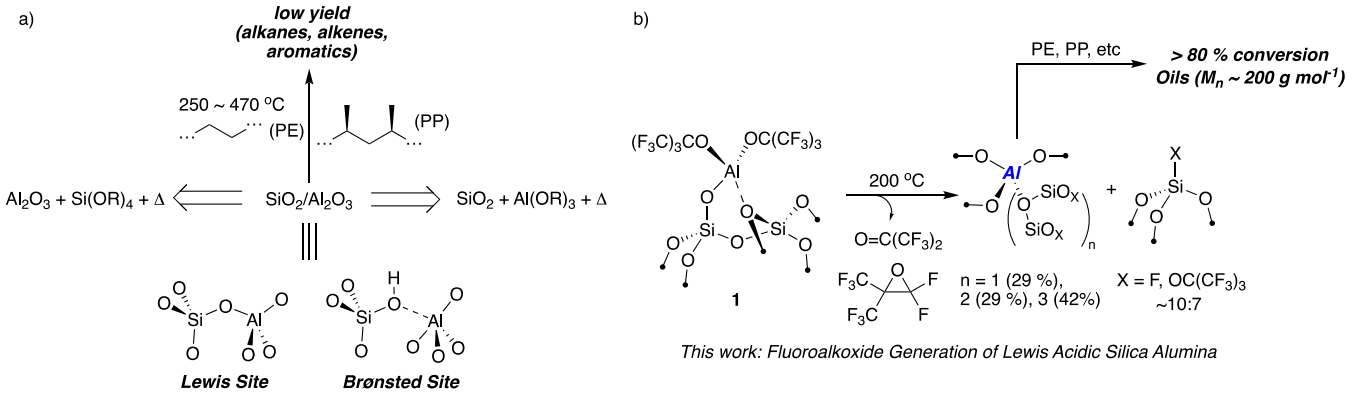

Figure 1. Traditional syntheses of amorphous silica–alumina (ASA) that perform poorly in reactions that crack polyethylene (PE) or isotactic polypropylene (iPP, a). Generation of fluorinated amorphous silica–alumina (F-ASA) through decomposition of the well-defined aluminum alkoxide (**1**, b). F-ASA is a competent catalyst for thermal cracking reactions of aliphatic polymers.

$mmol_{OH}\ g^{-1}$). After heating the mixture to 45 °C for 2 h, solid **1** was isolated by filtration and washed several times with PhF to remove residual $Al(OC(CF_3)_3)_3(PhF)$. The wet solid was dried under vacuum and stored in an Ar-filled glovebox freezer at −30 °C. Calcined $Al(OiPr)_3/SiO_2$[10c] and calcined $Al(TBOS)_3/SiO_2$[10b] were prepared as reported. Silica–alumina was purchased from Sigma-Aldrich and calcined at 500 °C under air for 4 h, followed by dehydroxylation under vacuum (10^{-5} mbar) at 500 °C for 12 h. $Al_2O_{3\text{-}500}$ and $Al_2O_{3\text{-}1000}$ were dehydroxylated under vacuum at 500 or 1000 °C, respectively. Compressed air was purchased from Airgas and was passed through a water trap (CRS, ZPure H_2O) immediately before use in calcinations. Low-molecular-weight iPP (M_w = 13.3 kDa; $Đ$= 2.4), high-molecular-weight iPP (M_w = 447.3 kDa; $Đ$= 5.5), and PVC (M_w = 133.0 kDa; $Đ$= 2.4) were purchased from Sigma-Aldrich and used as received. HDPE (DOW 17450 N, M_w = 142.1 kDa; $Đ$= 3.1) and ethylene/1-octene copolymer (DOW ENGAGE 8401, M_w = 288.7 kDa; $Đ$= 2.1) were purchased from commercial suppliers and used as received. Commercial plastics were collected from retailers and cut into small pieces by using a coffee grinder before use. All polymer properties used here are summarized in the Supporting Information (Table S3). Elemental analysis was performed at Atlantic Microlabs.

Solution ^1H and $^{13}C\{^1H\}$ NMR spectra were recorded on Bruker Avance 14.1 T ($\nu(^1H)$ = 600 MHz) spectrometers. FTIR spectra were recorded by using a Bruker Alpha IR spectrometer in an argon-filled glovebox. Solid-state NMR spectra acquired were recorded under magic angle spinning (MAS) at 14.1 T ($\nu(^1H)$ = 600 MHz) using a Bruker NEO600 spectrometer (UCR) or a Bruker Avance III spectrometer (Ames) and at 18.8 T ($\nu(^1H)$ = 800 MHz) using a Bruker AVANCE III spectrometer (UCSB). All solid-state NMR samples were packed and sealed in appropriately sized rotors in a glovebox under an inert atmosphere of Ar or N_2. Chemical shifts for all solid-state NMR spectroscopy experiments were referenced to the ^1H chemical shifts of neat tetramethylsilane using either adamantane (δ_{iso} = 1.82 ppm) or sodium trimethylsilylpropanesulfonate (δ_{iso} = 0.00 ppm) as a secondary reference. ^{13}C, ^{19}F, and ^{27}Al shifts were referenced by using previously reported IUPAC relative NMR frequencies. Solid-state 1D ^{19}F NMR experiments at UCR were performed at a 10 kHz spinning speed in 4 mm rotors sealed with Kel-F caps (Figure S14). Spectra were acquired using a rotor synchronized Hahn-echo pulse sequence ($\pi/2-\tau-\pi-\tau$–acq). Though Kel-F caps contain fluorine, control experiments showed that the signal from the cap only contributes a minor signal at −79 ppm that is distinct from ^{19}F resonances of F-ASA. Solid-state 1D ^{19}F NMR and $^{19}F\{^{27}Al\}$ symmetry-based Resonance-Echo Saturation-Pulse Double-Resonance (S-RESPDOR)[13] NMR experiments at Ames were carried out using a double-resonance Varian 1.6 mm fast-MAS probe configured to ^{19}F and ^{27}Al with a 33.333 kHz spinning frequency. The rotor was sealed with Torlon caps with Kel-F spacers between the cap and the sample. The Hahn-echo ^{19}F NMR spectrum shown in Figure 2a contains the same signals as those observed at slow-MAS obtained at the UCR, suggesting limited (if any) interference from the ^{19}F NMR signals in the Kel-F spacer in these experiments. Hard ^{19}F pulses were applied with a 78 kHz radiofrequency power. 2048 scans were accumulated for both experiments with the recycle delay set to 5 s. S-RESPDOR data were fitted using INTERFACES software.[14]

EDS elemental mapping was recorded on a Thermo Fisher Scientific Titan Themis 300 SEM instrument. Gas-phase GC analyses were performed on an Agilent 7820 GC containing a flame ionization detector (FID) using an HP-PLOTQ column or a thermal conductivity detector (TCD) using CP-Molsieve 5A (H_2 and CO_2 quantification). For FID, the oven was held at 150 °C for 10 min; 200 μL of the gas sample was injected using a split ratio of 76.926:1. The temperature of FID was set at 350 °C and N_2 was used as the carrier gas. The flow rate was 23.7 mL/min. The flow rates of air and hydrogen were set to 400 and 30 mL/min, respectively. For GC-TCD, the GC column oven was held at 80 °C for 5 min, 200 μL of the gas sample was injected using a split ratio of 5:1. The temperature of TCD was set at 200 °C and N_2 was used as the carrier gas with a 3.5 mL/min flow rate. The flow rate of air was set at 10 mL/min. Note, the TCD detector is very sensitive to fluorocarbons and gases contaminated with fluorocarbons result in irreversible deactivation of the detector. Descriptions of gas quantification are described in the Supporting Information. Liquid-phase GC analyses were performed on an Agilent 7820 GC containing a flame ionization detector (FID) using an HP-5 column; the GC column oven was held at 50 °C for 3 min, and the temperature was subsequently raised to 300 °C (10 °C/min) and held at this temperature for 10 min. 5 mL of the liquid sample was injected, and the split ratio was 10:1. The temperature of FID was set at 350 °C and N_2 was used as the carrier gas and the flow rate was 25 mL/min. The flow rate of air and hydrogen were set to 400 mL/min and 30 mL/min, respectively.

For liquid-phase GC quantification, due to the complexity of the products, we assume that all hydrocarbon products (alkanes, alkenes, and aromatics) have the same per-carbon response factor. As a result, we can integrate all peaks as a whole and use a known amount of tetradecane as an internal standard.

Room-temperature GPC was performed on TOSOH SEC using HPLC grade THF as the mobile phase. Samples were injected at a concentration of 1 mg mL^{-1} and filtered through a 0.25 μm PTFE filter prior to analysis. The GPC calibration curve was constructed using polystyrene for high molecular weights and linear alkanes for low molecular weights (Figure S3). High-temperature GPC was performed on an Agilent 1260 Infinity II instrument that incorporates a differential refractive index detector. HPLC grade 1,2,4-trichlorobenzene (TCB) was used as the mobile phase at a flow rate of 1 mL min^{-1}. Columns and detectors were maintained at 140 °C. All polymers were injected at a concentration of 1 mg/mL and filtered through a 0.2 μm PTFE filter prior to analysis. Calibration was made using polystyrene standards that were corrected for linear poly-

https://doi.org/10.1021/jacs.5c04524
J. Am. Chem. Soc. 2025, 147, 18145−18154

ethylene or polypropylene by universal calibration using the Mark−Houwink parameters.

Preparation of F-ASA. In an argon-filled glovebox, **1** (250 mg, 0.05 mmol of Al) was placed into a 25 mL flask containing a Teflon tap. The flask was sealed, taken out of the glovebox, and connected to a short path distillation apparatus containing an empty oven-dried 50 mL flask containing a Teflon tap, as shown in Figure S4. The apparatus was placed under high vacuum, while keeping the flask containing **1** sealed, for 3 min, and then the flask containing **1** was opened to vacuum for another 3 min. The Teflon tap was connected to the short path, the center tap as shown in Figure S4 was sealed to maintain a static vacuum in the system. The flask containing **1** was heated at 200 °C while the 50 mL bottle was submerged in liquid nitrogen to capture all volatiles produced during thermolysis. After 2 h, the two flasks were sealed. The flask containing **1** was disconnected from the short path and taken into an argon-filled glovebox for further analysis. A J. Young NMR tube containing C_6D_6 (0.5 mL) and trifluorotoluene (12.3 μL, 0.1 mmol), which was freeze−pump−thawed 3 times to ensure removal of gases, was connected to the short path. The short path was placed under a vacuum for 5 min. The Teflon tap was connected to the short path, the center tap as shown in Figure S3 was sealed to maintain static vacuum in the system. The NMR tube was immersed in liquid nitrogen, the tap on the NMR tube was opened, and finally the tap containing volatiles was opened. This procedure transferred the volatiles to the NMR tube. Quantification of volatiles was performed using ^{19}F NMR with trifluorotoluene as the internal standard. NMR characterization of the volatiles is shown in Figures S5−S7. GC-TCD analysis of the gas phase as depicted in Figure S8 shows that CO_2 is formed in this reaction. F-ASA was collected as a dark brown solid and was stored in an Ar glovebox. FTIR data of F−ASA are shown in Figure S10 and solid-state NMR characterization is shown in Figures S12−S17. Elemental analysis: 2.22% F (1.2 mmol g^{-1}). SEM-EDS analysis (Figure S18) gives a fluorine loading of 1.8%. ^{29}Si{^{1}H} MAS NMR (119 MHz, 5 kHz): −109 (SiO_2), −112 (SiO_2) ppm. ^{29}Si{^{19}F} MAS NMR (119 MHz, 10 kHz): −96 ($O_{2/2}$ SiF_2), −99 (SiO_2), −106 ($O_{3/2}$ SiF), and −110 (SiO_2). ^{1}H MAS NMR: 7.0 (PhF or Brønsted acid sites), 1.8 (SiOH), and 1.1 (SiOH) ppm. ^{19}F MAS NMR (564 MHz, 10 kHz): −70.6 (Si−CF_3); −75.6 (Si−CF_3); −156.7 (Si−F); −164 (Si−F) ppm. ^{13}C{^{19}F} MAS NMR (151 MHz, 10 kHz): 120 (CF3); 119 (CF3); and 78 ($C(CF_3)_3$. The integrated Si−CF_3: Si−F is 10:7. ^{27}Al{^{1}H} MAS NMR (156 MHz, 18.8 kHz): δ_{iso} 45 (Al^{IV}), 33 (Al^{V}), and −5 (Al^{VI}) ppm.

Pyridine Contact Experiments. F-ASA (0.2 g, 0.04 mmol Al) and 5 mL of pentane were transferred to a 25 mL Schlenk flask containing a Teflon tap and a side arm inside an argon-filled glovebox. The flask was removed from the glovebox, connected to a high vacuum line, cooled to 77 K with liquid nitrogen, and evacuated for 5 min. Dried and degassed pyridine was vacuum transferred into the bottle at 77 K and the mixture was gently stirred at room temperature for 1 h. After this time, the unreacted pyridine and pentane were removed under vacuum and the solid was dried under diffusion pump vacuum for 45 min. The resulting solid was collected and stored in an Ar glovebox. ^{15}N{^{1}H} CPMAS NMR (61 MHz, 10 kHz): 260, 202 ppm. ^{27}Al Hahn-echo NMR (156 MHz, 10 kHz): 49.4, 4.2 ppm.

Triethylphosphine Oxide (TEPO) Contact Experiments. F-ASA (0.500 g, 0.10 mmol of Al) and various molar equivalents (0.25, 0.5, 0.75, and 1.1) of TEPO were transferred into separate arms of a double-Schlenk flask inside an argon-filled glovebox. The flask was removed from the glovebox, connected to a high vacuum line, and evacuated for 5 min. Pentane (∼5 mL) was condensed into the side of the flask containing TEPO at 77 K, and the clear colorless solution was filtered to the other side of the double-Schlenk onto F-ASA. The mixture was warmed to room temperature and gently stirred for 4 h at room temperature. After this time, the clear colorless solution was filtered on the other side of the double-Schlenk flask. The arm of the double-Schlenk flask containing TEPO contacted with F-ASA was cooled to 77 K, causing the pentane on the other side of the flask to condense onto the functionalized silica. The pentane was warmed to 25 °C, stirred for 5 min, and filtered back to the other side of the double Schlenk. This procedure was repeated two more times to remove unreacted TEPO from the functionalized silica surface. The volatiles were removed under vacuum, and the solid was dried under diffusion pump vacuum for 45 min. The resulting solid was collected and stored in an Ar glovebox.

Preparation of HF-Etched SiO_2/Al_2O_3. In a 50 mL plastic centrifuge tube, 5 g of silica−alumina was mixed with 10 mL of DI water, and 5 mL of 3% HF acid was added dropwise. The mixture was stirred at room temperature overnight, followed by drying at 120 °C for 4 h. The dried material was then calcined at 500 °C in a quartz tube under air for 4 h. After this time the tube was sealed, and the material was placed under vacuum at 500 °C for 13 h. The quartz tube was cooled to room temperature, transferred into an argon glovebox, and stored at room temperature. ^{19}F MAS NMR (564 MHz, 10 kHz): −154 ppm (Si−F).

General Procedure for Polymer Breakdown. The catalytic reaction was conducted in a 100 mL Parr reactor (Figure S28). In a typical reaction, a polyolefin (5 g iPP or 1g HDPE or Engage) and **F-ASA** (300 mg) were loaded into the autoclave in an Ar-filled glovebox. The autoclave was removed from the glovebox and heated at the desired temperature for a designated time. After the system was cooled using a high flow of compressed air, the Parr reactor was connected to an under-vacuum bottle. The volatiles were taken from the bottle and analyzed by GC. At this point, the flask was opened to ambient atmosphere for extraction of oils from this mixture. CH_2Cl_2 was added to the flask at room temperature, and the solution was decanted from the remaining solid. This procedure was repeated three more times. The combined CH_2Cl_2 extract was then separated into low-boiling-point products and high-boiling-point products by vacuum distillation at room temperature.

Large-Scale Pyrolysis Reactions. In a typical reaction, a polyolefin (50 g) and F-ASA (1 g) were loaded into the distillation apparatus as shown in Figure S48 in an Ar-filled glovebox. The system was removed from the glovebox and connected to a vacuum line with a rubber hose. The apparatus was evacuated and heated at the temperature for a designated time, as shown in Table S10. The system was occasionally opened to vacuum every 20−30 min to aid distillation of the oil into the receiving flask. After the reaction, the system was disconnected, and the oil was weighed. This yield is the "low boiling liquid" shown in Table S10. DCM (30 mL) was added to the flask containing polymers to obtain higher-molecular-weight products. The exact DCM solution was evaporated, and the heavier product was weighed. This fraction is referred to as "high boiling point" in Table S10. Under these conditions, light gases were not recovered.

RESULTS

Generation of F-ASA. Thermolysis of **1** (0.20 $mmol_{Al}$ g^{-1}) at 200 °C forms F-ASA and a small amount of hexafluoroacetone (0.02 mmol g^{-1}) and the epoxide of perfluoroisobutene (0.08 mmol/g) as shown in Figure 1b. The organic products formed in this account for ∼25% of the Al−OR^F in **1**. The remainder of Al-OR^F decomposes to CO_2, which is detected in the gas phase (Figure S9). The mechanism of this process is not known. Combustion analysis of F-ASA gives 2.22% F (1.2 $mmol_F$ g^{-1}), indicating that some fluoride remains in the material after thermolysis.

The ^{19}F magic angle spinning (MAS) nuclear magnetic resonance (NMR) spectrum of F-ASA contains a broad signal at −157 ppm (Si−F) and a sharp signal for Si−$OC(CF_3)_3$ at −76 ppm, as shown in Figure 2a. The ^{27}Al MAS NMR spectrum of F-ASA is shown in Figure 2b and contains signals for Al^{IV} (29%), Al^{V} (29%), and Al^{VI} (42%). These signals are uniformly shifted by ∼20 ppm to lower frequency when compared to Al_2O_3,[15] suggesting that these are isolated sites with Al−O−Si linkages. Figure 2c shows results from ^{19}F{^{27}Al} symmetry-based Resonance-Echo Saturation-Pulse Double-Resonance

https://doi.org/10.1021/jacs.5c04524
J. Am. Chem. Soc. 2025, 147, 18145−18154

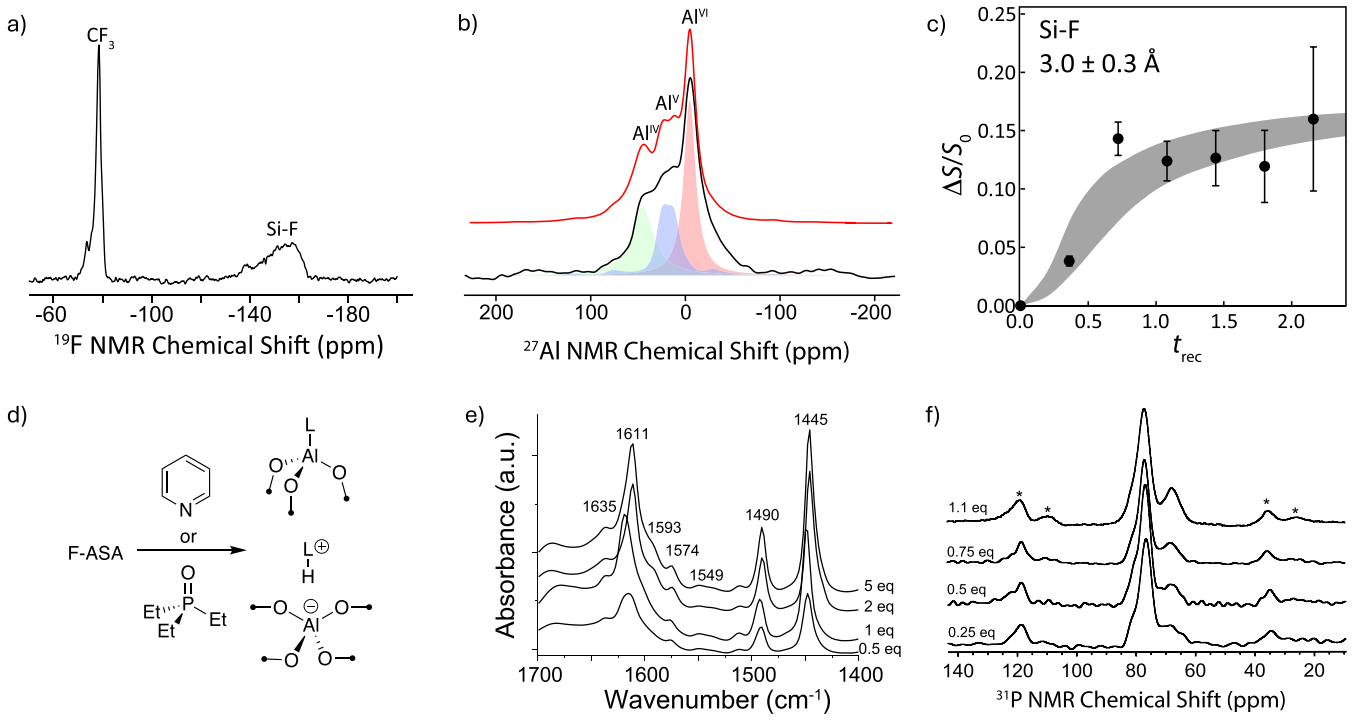

Figure 2. ^{19}F fast MAS NMR spectrum of F-ASA (a). ^{27}Al MAS NMR spectrum of F-ASA (b). The experimental spectrum in (b) is shown in black, the full simulation of the spectrum is in red. The light shaded signals in green, blue, and red are simulated intensities for the Al(IV), Al(V), and Al(VI) sites, respectively. $^{19}F\{^{27}Al\}$ S-RESPDOR dephasing curve for the Si−F resonance of F-ASA (c). Reactive probes to determine acid site distribution in F-ASA (d). FTIR spectra of pyridine adsorbed onto F-ASA (e). $^{31}P\{^{1}H\}$ MAS NMR data of F-ASA contacted with triethylphosphine oxide (f). The spectrum in (a) and the dephasing curve in (c) were recorded at 14.1 T with ν_{rot} = 33.333 kHz. The spectrum in (b) was recorded at 18.8 T with ν_{rot} = 18.87 kHz.

(S-RESPDOR)[13,16] experiments of F-ASA. This experiment introduces dipolar coupling between nearby aluminum and fluorine spins that results in ^{19}F signal dephasing, the rate of which depends on the F−Al internuclear distance. The S-RESPDOR dephasing curve plateaus at ∼20%, indicating that most of the surface fluorine are far (>7 Å) from aluminum. Those that are close to aluminum have a 3.0 ± 0.3 Å Al−F distance, which is outside the covalent radii of these elements and near the limit of the van der Waals radii (∼3.31 Å), suggesting minimal interaction between Al and F in F-ASA. The S-RESPDOR dephasing curve for the signal from $-CF_3$ groups also shows that aluminum is far from these sites (Figure S14c), though this could also be due to dynamic averaging of the $-CF_3$ on the S-RESPDOR time scale.

Both pyridine and triethylphosphine oxide adsorption indicate that F-ASA contains Brønsted and Lewis sites, as shown in Figure 2d. Excerpts of the Fourier transform Infrared (FTIR) spectra of F-ASA contacted with various amounts of pyridine are shown in Figure 2e. These spectra contain minor bands at 1549 and 1635 cm^{-1} from adsorbed pyridinium and bands at 1445, 1490, 1574, and 1611 cm^{-1} from Lewis adducts of pyridine and aluminum in F-ASA. Consistent with this analysis, the $^{15}N\{^{1}H\}$ CPMAS NMR spectrum of F-ASA contacted with ^{15}N-pyridine contains signals at 201 ppm for pyridinium and 260 ppm for pyridine bound to Lewis sites (Figure S20).

Triethylphosphine oxide (TEPO) binds stronger to Lewis sites than pyridine[17] and is a complementary probe that is often used to study acidity on surfaces using ^{31}P MAS NMR.[18] The $^{31}P\{^{1}H\}$ MAS NMR spectrum of F-ASA contacted with various amounts of TEPO is shown in Figure 2f. These spectra contain signals at 77 ppm assigned to TEPO interacting with Lewis sites and signals at 68 ppm assigned to TEPO interacting with Brønsted sites. The integrated intensity of these peaks is ∼10:1 Lewis/Brønsted, and is consistent with pyridine adsorption data showing that Lewis sites are the major species in F-ASA. The change in ^{31}P NMR chemical shift ($\Delta\delta(^{31}P)$) reports the strength of Lewis acids.[19] The $\Delta\delta^{31}P$ values from strong Lewis sites are 27 ppm. The $\Delta\delta(^{31}P)$ of **1** contacted with TEPO is 28 ppm,[12b] indicating that the Lewis sites in F-ASA are of similar strength as the well-defined aluminum site in **1**. Although F-ASA contains Al(IV), Al(V), and Al(VI) sites; the ^{27}Al MAS NMR spectra of F-ASA in contact with either pyridine or TEPO show pronounced increases in tetrahedral Al(IV) sites and decreases in Al(VI) sites. This result suggests that the aluminum sites rearrange when contacted with these substrates and implies that the aluminum sites in F-ASA are accessible to substrates.

Figure 3 shows representative data for the F-ASA breakdown of high-molecular-weight iPP (M_w = 447.3 kDa; $Đ$= 5.5). A neat melt of polymer with F-ASA at a very low catalyst loading (6 wt %, ∼2000 monomer/Al, 0.05 mol % Al) forms an oil that is soluble in hydrocarbon solvents with the complex microstructure shown in Figure 3a. The conversion and selectivity versus time are plotted in Figure 3b. F-ASA also produces a small amount of light gas or liquid alkanes/alkenes ($C_1 \sim C_9$). The minor gaseous products contain mostly butenes, although small amounts of propene, propane, and C_5 products are also formed. Only traces of methane and ethane are in the gas phase. H_2 also forms in the reaction, reaching a maximum of ∼3 equiv of H_2 per aluminum after 6 h.

https://doi.org/10.1021/jacs.5c04524
J. Am. Chem. Soc. 2025, 147, 18145−18154

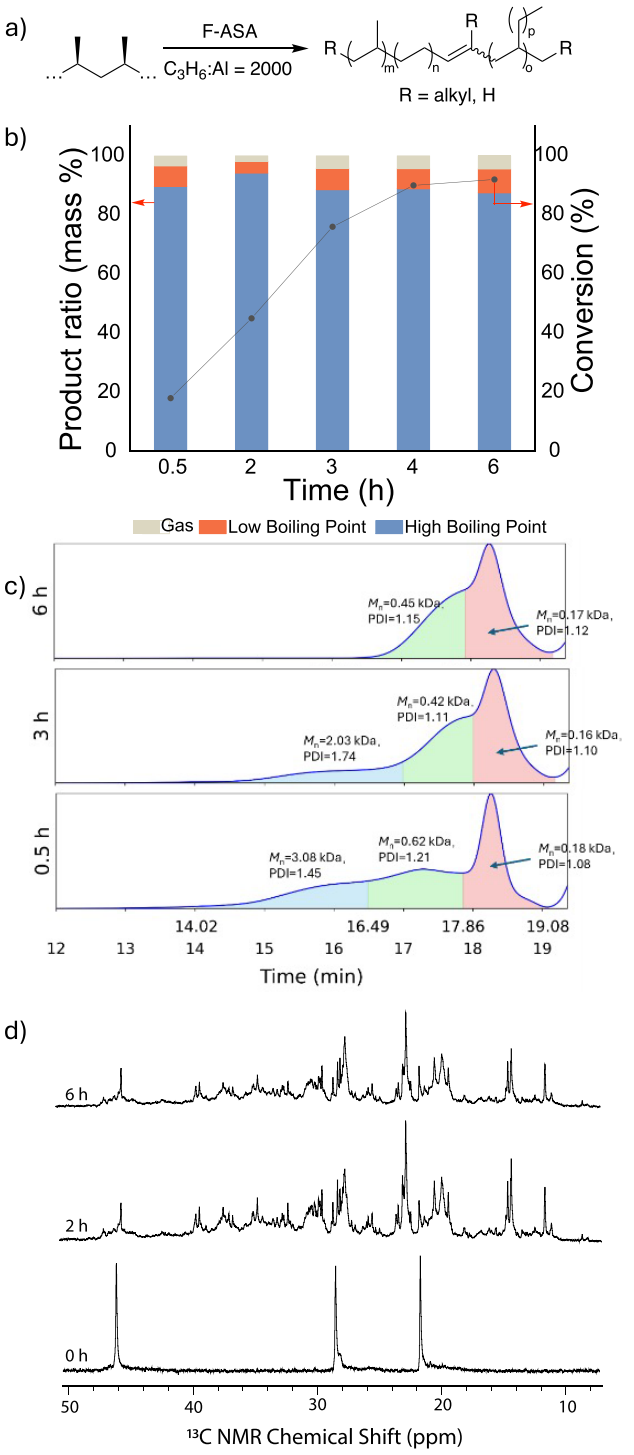

Figure 3. Breakdown of iPP with F-ASA (a). Product and conversion versus time (b). GPC data of oils (c). $^{13}C\{^1H\}$ NMR data of oils (d). PDI = polydispersity index = $Đ$.

Time-resolved GPC data of the oil are shown in Figure 3c. At short reaction times, moderately high-molecular-weight products (M_n = 3.1 kDa, $Đ$ = 1.45; M_n = 0.6 kDa, $Đ$= 1.2) are present in the chromatograms. As the reaction progresses these products are consumed, and lower-molecular-weight products are formed until a bimodal molecular weight distribution is obtained. The lowest-molecular-weight fraction from this experiment has M_n ~ 0.17 kDa and $Đ$= 1.12, corresponding to an average chain length of ~14 carbons for the lowest-molecular-weight fraction.

The $^{13}C\{^1H\}$ NMR spectra of iPP and the oils produced at 2 and 6 h reaction times are shown in Figure 3d. Independent of the reaction time, F-ASA produces oils that have essentially identical, yet extraordinarily complex microstructures. This complex signal pattern is characteristic of complete loss of diastereoselectivity from the iPP and formation of regioirregular errors that resemble hyperbranched random ethylene-propylene copolymers.[20] However, analysis of the unreacted polymer shows minimal degradation of <*mmmm*> tetrads (Figure S33). The oils from this reaction contain ~2% olefins as mostly internal di- and trisubstituted olefins (major, ~86%) and terminal vinylidene signals (minor, ~14%). Signals for terminal α-olefins are not observed. ^1H NMR signals for aromatics, which are known to form in pyrolysis reactions,[6b,21] are also present in low quantities (0.2%).

F-ASA shows broad-spectrum reactivity toward aliphatic polymers to form branched oils as the major product of the reaction. The yields from these reactions are summarized in Figure 4a. Detailed characterization of the oils generated in these reactions is given in the Supporting Information. Low-molecular-weight iPP (M_n = 13.3 kDa, $Đ$= 2.4) forms branched oils in 83% yield, similar to the results shown in Figure 3. At lower F-ASA loading (2 wt %, Monomer/Al = 6000), oils form in 68% yield. At 3000:1 monomer/Al loading, F-ASA converts this iPP to oils in 78% yield. Isolation of the catalyst after the reaction gives a black powder (Figure S52) indicating that the catalyst contains coke after the polymer breakdown reaction. However, analysis of the coked catalyst by ^{27}Al MAS NMR contains signal patterns essentially identical to those of fresh F-ASA (Figure S54). Calcination of spent F-ASA at 500 °C removes the coke and regenerates the catalyst. Over two subsequent recycles, F-ASA converts low-molecular-weight iPP to oils in 80% and 69% yields, respectively.

F-ASA is superior in this reaction compared to other closely related materials. Aluminum oxide partially dehydroxylated at 1000 °C (Al_2O_{3-1000}), a material that contains strong Lewis sites capable of activating C−H bonds,[22] shows poor reactivity in PP breakdown, resulting in only 2% isolated yield of branched oils. Commercially available SiO_2/Al_2O_3 or ASAs generated from either $Al(TBOS)_3$ (TBOS = tri(*tert*-butoxy)-siloxy)[10b] or $Al(O^iPr)_3$[11a] also show poor reactivity toward PP in this reaction. HF-treated SiO_2/Al_2O_3 performs somewhat better in this reaction, forming oils in 18% yield.

Melts of ethylene/1-octene copolymer (ENGAGE) or high-density PE (HDPE) also react with F-ASA to form branched oils as the major product, though higher catalyst loadings are required to achieve yields >70% of oils in a single run. Dropping F-ASA loading to 5500:1 in HDPE degradation reaction results in a 34% yield of hyperbranched oils (B/1000 C = 180). This reactivity data infer a general reaction trend of iPP > ethylene/1-octene copolymer ~ HDPE in terms of yield of oil.

F-ASA also breaks down common postconsumer plastics shown in Figure 4b to branched oils. The trends that emerge are very similar to those described above for the virgin polymers. The reactivity of the various polymers, in terms of yield of oil, follows the trend PP > LLDPE ~ LDPE > HDPE. Purposely adding 10 wt % PVC to the PP water cup only marginally reduces yields in the polymer breakdown reaction, indicating that F-ASA is compatible with this common

https://doi.org/10.1021/jacs.5c04524
J. Am. Chem. Soc. 2025, 147, 18145−18154

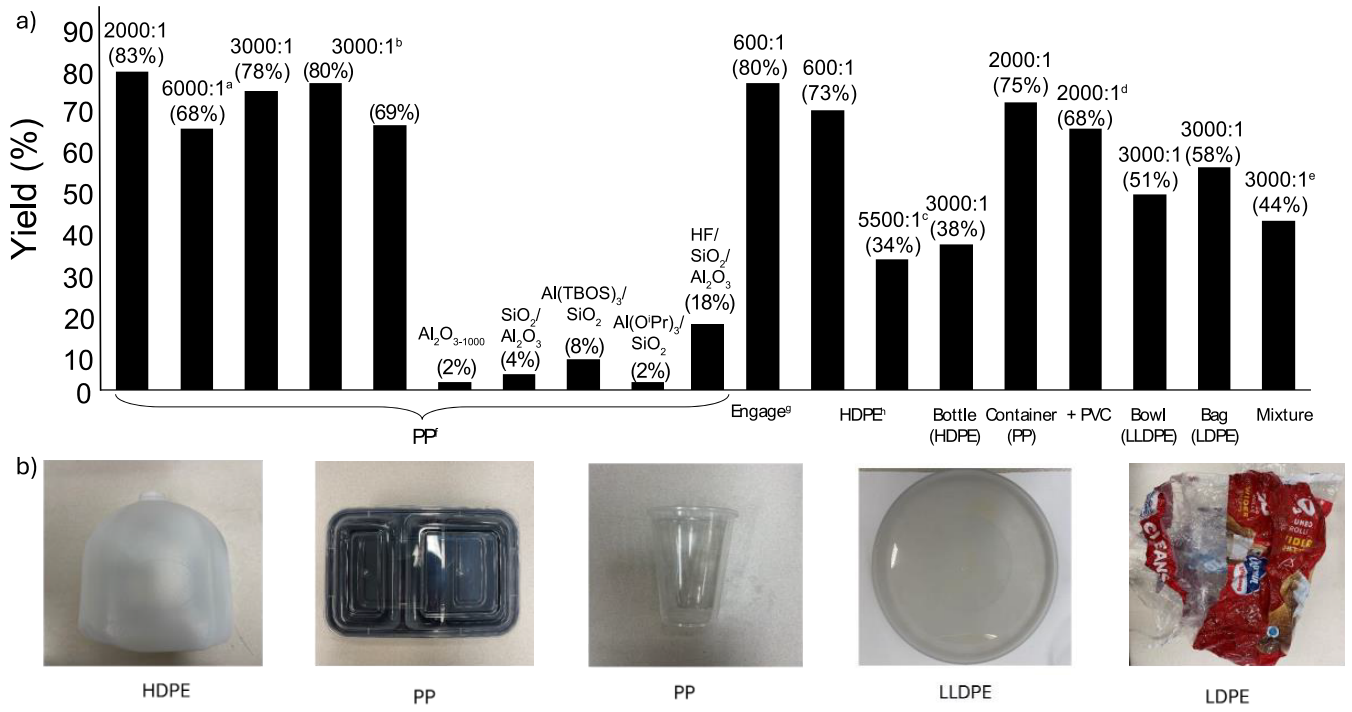

Figure 4. Yield of oil from various polymer breakdown reactions with F-ASA (a). Pictures of commercial polymers that react with F-ASA (b). The numbers given over the bars in (a) are the monomer/Al ratios. Unless noted otherwise, reactions were run at 250−300 °C as neat melts. [a]—330 °C; [b]—recycled by calcining the spent catalyst under air at 500 °C; [c]—370 °C; [d]—contains 10 wt % PVC; [e]—contains HDPE, PP, LDPE, LLDPE; [f]—M_n = 13.3 kDa, $Đ$= 2.4; [g]—ethylene/1-octene (Engage) copolymer (M_n = 140.1 kDa, $Đ$= 2.1); [h]—M_n = 49.1 kDa, $Đ$= 5.7, B = 5/1000 C.

impurity that acts as a poison to many catalysts in these types of reactions.

In addition to the broad plastic substrate scope and recyclability, F-ASA is scalable to some extent. Using a relatively straightforward distillation apparatus (Figure S48), 1 g of F-ASA in a melt of 50 g of neat iPP (M_n = 13.3 kDa, $Đ$= 2.4) forms distilled oils in 68% yield with a heavy extractable fraction formed in 10% yield. The spectroscopic properties of these oils are similar, but the heavier fraction contains higher-molecular-weight waxes. Similar properties are obtained with high-molecular-weight iPP, HDPE, Engage, and the commercial food container as shown in Figure 4b. These results are summarized in Table S8 of the Supporting Information.

■ DISCUSSION

Selected strategies to chemically process HDPE are shown in Figure 5. High-temperature pyrolysis forms pyrolytic crude oil in moderate yields.[23] Uncatalyzed pyrolysis requires >415 °C to begin break down of HDPE or above 355 °C to initiate pyrolysis of PP, temperatures far below what is required to pyrolyze or crack small molecule alkanes in the absence of catalysts. These reactions probably involve free radicals that cleave polymer chains.[24] The high operating temperature in pyrolysis reactions also results in complex unselective reactions that form aromatics that can complicate downstream processing of the pyrolysis oil.

Basset and Dufaud showed that Zr−H supported on silica polymerizes ethylene and depolymerizes polyethylene in the presence of H_2.[25] This reaction generates a distribution of linear alkanes, ultimately converging to a mixture of methane and ethane at a high conversion. During the past several years, this reaction re-emerged more broadly in hydrogenolysis of polymers. For example, [Zr−H$^+$][26] or [Ta−H$^+$][25−27] sites

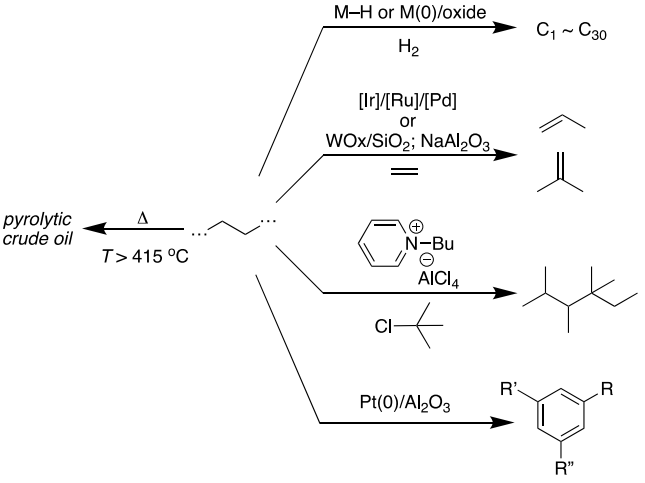

Figure 5. Selected reactions that chemically break down HDPE.

supported on sulfated oxides are more reactive than hydrides supported on silica in this reaction. Alternatively, intermediates in the catalytic cycle can be intercepted by alkylaluminum reagents for further chemical elaboration.[28] Supported noble metal nanoparticles[29] or ZrO_2 nanoparticles[30] also catalyze hydrogenolysis of HDPE.

Selected strategies that do not involve hydrogen are also listed in Figure 5. For example, mixtures of Ir-, Pd-, and Ru-complexes catalyze orthogonal reaction chemistries that dehydrogenate the polymer, isomerize the olefin, and ultimately cleave chains through ethenolysis.[31] These reactions form propylene as a major product with molecular catalysts and mixtures of propylene and isobutene with heterogeneous catalysts. Ionic liquids containing chloroalkanes cleave C−C

https://doi.org/10.1021/jacs.5c04524
J. Am. Chem. Soc. 2025, 147, 18145−18154

bonds in HDPE into liquid branched alkanes by forming carbocations that crack to form alkanes and alkenes that are subsequently alkylated.[32] Oxidative processes produce mixtures of carboxylic acids that are subsequently metabolized by organisms to functionalized organic molecules.[33] Finally, $Pt(0)/Al_2O_3$ forms long-chain aromatics from PE.[21]

F-ASA-catalyzed pyrolysis is complementary to these methods. The most attractive feature of F-ASA is that this catalyst does not require an additional reagent to drive the reaction. The conditions for chain cleavage are similar to those using $Pt(0)/Al_2O_3$, but aromatics are not formed as readily with F-ASA. Instead, highly branched alkanes form, even from linear HDPE. In that case, F-ASA forms a branched oil containing 181 branches per 1000 C from an HDPE material containing less than 3 branches.

The formation of internal olefins and branches provides some explanation for how a reaction that is clearly thermochemically unfavorable can become favorable. Scheme 1 shows calculated ΔG for *n*-undecane cleavage at 300 °C.

Scheme 1. Calculated ΔG for *n*-Undecane Cracking at 300 °C Using Values from NIST

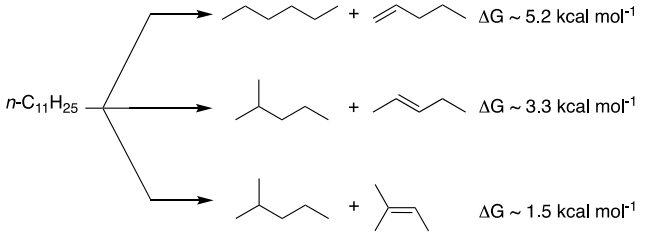

Cleavage to form *n*-hexane and 1-pentene is quite unfavorable, but including one branch in the C_6 fragment and isomerizing the terminal olefin to internal reduces overall ΔG by ~2 kcal mol^{-1}. Increasing branching and substitution of the olefin in the C_5 fragment renders the reaction more favorable than the linear case by 3.7 kcal mol^{-1}. These values are obviously imperfect. Liquid *n*-undecane hardly approximates an aliphatic polymer melt, but these values provide a simple explanation to support the observations that polymers cleave thermally in catalytic reactions with F-ASA.

There are a couple of mechanistic questions involving F-ASA that warrant limited commentary. Fluorinated alumina is often prepared by treating an oxide with HF, $CClF_3$, or alkyl fluorides.[34] Nanoscopic AlF_xO_{3-x} are also available through nonaqueous sol–gel methods.[35] In **1**, the $Al-OR^F$ fragment thermally decomposes to F-ASA. This chemistry is related to thermolytic molecular precursors, a class of compounds containing thermally sensitive ligands that controllably decompose to form materials or single sites supported on oxides.[36] Though $Al(OC(CF_3)_3)_3$ is not expected to behave as a thermolytic molecular precursor, Krossing and co-workers showed that base-free $Al(OC(CF_3)_3)_3$ eliminates the epoxide of perfluoroisobutene,[37] the same epoxide detected in thermolysis of **1**, and shows that there is a relatively low barrier process to controllably decompose the $-OC(CF_3)_3$ ligand.

Thermolysis of $Al-OR^F$ in **1** is clearly more complex because a significant fraction of the $-OC(CF_3)_3$ ligand decomposes to CO_2 and Si–F. This suggests a rather complicated sequence of mechanistic steps that formally transfers C–F bonds to Si–O–Si to form Si–F and eventual transfer of oxygen to carbon to form CO_2. The exact sequence of steps that led to these products is unknown. Though mechanistic information is limited, descriptions of fluoroalkane decomposition on silica date to at least the 1960s.[38] $O{=}CF_2$ or CO, common intermediates in fluorocarbon decomposition reactions, was not detected under the conditions reported here.

The reactive intermediate(s) that result in chain cleavage are also not known. It is tempting to ascribe most, or all, of this behavior to the acidic sites present on F-ASA. Carbocations in ASAs or crystalline zeolites form from reactions of Brønsted or Lewis sites,[39] and F-ASA and related fluorinated alumina contain both. In polymer melts, when a carbocation forms, β-scission reactions are proposed to cleave C–C bonds of the main chain.[17]

A more provocative explanation may lie in studies performed by McVicker, Kramer, and Ziemiak in cracking reactions of isobutane using zeolites and halogenated aluminas.[40] Zeolites show typical selectivity profiles from carbocation-based cracking reactions. However, halogenated aluminas produce far more isobutene, propene, and methane. These products were proposed to form from reactions of "defect" sites and isobutane to form alkyl radical cations. Though alkyl radical cations are obviously reactive,[41] and isobutane radical cations are expected to form methane and propene, this proposal is unlikely. The vertical ionization potential for isobutane is 10.7 eV, a value far higher than reasonably accessible on a redox inactive oxide.[42] An alternative explanation is the formation of an isobutyl radical after a hydrogen atom abstraction (or proton-coupled electron transfer) by the defect site,[43] shown in eq 1 for a putative oxygen-centered defect site. Thermal

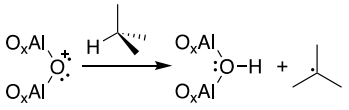

(1)

cracking of isobutane through radical intermediates also forms isobutene, propene, and methane with similar selectivity to those studied by McVicker, Kramer, and Ziemiak.[44] If similar chemistry occurs with F-ASA will require further study, but a similar reaction could explain the efficiency of F-ASA in initiating the polymer breakdown reactions presented here.

CONCLUSION

A well-defined silica–alumina material containing a strong Lewis acid site thermally decomposes to fluorinated silica–alumina (F-ASA). This material contains both Lewis acidic aluminum and Brønsted acid sites. A number of aliphatic polymer melts (250–300 °C) react with F-ASA at low catalyst loading to form branched hydrocarbon oils in good yields. Catalyst loadings as low as 2 wt % (0.017 mol % aluminum) are accessible. The oils contain olefins for further chemical elaboration and form only a small amount of aromatics. The low aromatic quantity of aromatics is probably related to the much lower temperature of F-ASA-mediated pyrolysis compared to that of uncatalyzed pyrolysis and the absence of a transition metal that can reversibly dehydrogenate and cyclize paraffins more readily. The mechanistic questions raised here require further study, which is currently underway.

https://doi.org/10.1021/jacs.5c04524
J. Am. Chem. Soc. 2025, 147, 18145–18154

■ ASSOCIATED CONTENT

Supporting Information

The Supporting Information is available free of charge at https://pubs.acs.org/doi/10.1021/jacs.5c04524.

FTIR spectra, solid-state NMR spectra, gas chromatograph traces, solution NMR spectra of extracted oils, and characterization data of polymers (PDF)

■ AUTHOR INFORMATION

Corresponding Author

Matthew P. Conley − *Department of Chemistry, University of California, Riverside, California 92507, United States;* orcid.org/0000-0001-8593-5814; Email: matthew.conley@ucr.edu

Authors

Jiaxin Gao − *Department of Chemistry, University of California, Riverside, California 92507, United States*

Frédéric A. Perras − *Chemical and Biological Sciences Division, Ames National Laboratory, Ames, Iowa 50011, United States; Department of Chemistry, Iowa State University, Ames, Iowa 50011, United States*

Complete contact information is available at: https://pubs.acs.org/10.1021/jacs.5c04524

Notes

The authors declare the following competing financial interest(s): A patent was filed describing this technology.

■ ACKNOWLEDGMENTS

M.P.C. is a member of the UCR Center for Catalysis. This work was funded by the U.S. Department of Energy (DOE), Office of Basic Energy Sciences, Division of Chemical Sciences, Geosciences, and Biosciences under DE-SC0025290 (M.P.C.). Solid-state NMR work at Ames (F.A.P.) was supported by the U.S. Department of Energy (DOE), Office of Basic Energy Sciences, Division of Chemical Sciences, Geosciences, and Biosciences, Catalysis Science program. Ames National Laboratory is operated for the DOE by Iowa State University under Contract No. DE-AC02-07CH11358. We thank Dr. Lingchao Zhu for $^{13}C\{^{19}F\}$ CP solid-state NMR setup. We are grateful for Prof. William Neary at UC Riverside for providing access to a room-temperature GPC. We also thank Dr. Tiantian Zhou for developing a Python program to process the GPC data.

■ REFERENCES

(1) (a) Coates, G. W.; Getzler, Y. D. Y. L. Chemical recycling to monomer for an ideal, circular polymer economy. *Nat. Rev. Mater.* **2020**, *5*, 501−516. (b) Kosloski-Oh, S. C.; Wood, Z. A.; Manjarrez, Y.; de los Rios, J. P.; Fieser, M. E. Catalytic methods for chemical recycling or upcycling of commercial polymers. *Mater. Horiz.* **2021**, *8*, 1084−1129.

(2) Schyns, Z. O. G.; Shaver, M. P. Mechanical Recycling of Packaging Plastics: A Review. *Macromol. Rapid Commun.* **2021**, *42*, 2000415.

(3) Sun, J.; Dong, J.; Gao, L.; Zhao, Y.-Q.; Moon, H.; Scott, S. L. Catalytic Upcycling of Polyolefins. *Chem. Rev.* **2024**, *124*, 9457−9579.

(4) (a) Zones, S. I. Translating new materials discoveries in zeolite research to commercial manufacture. *Microporous Mesoporous Mater.* **2011**, *144*, 1−8. (b) Busca, G. Acid Catalysts in Industrial Hydrocarbon Chemistry. *Chem. Rev.* **2007**, *107*, 5366−5410. (c) Corma, A. Inorganic Solid Acids and Their Use in Acid-Catalyzed Hydrocarbon Reactions. *Chem. Rev.* **1995**, *95*, 559−614.

(5) Serrano, D. P.; Aguado, J.; Escola, J. M. Developing Advanced Catalysts for the Conversion of Polyolefinic Waste Plastics into Fuels and Chemicals. *ACS Catal.* **2012**, *2*, 1924−1941.

(6) (a) Ishihara, Y.; Nambu, H.; Ikemura, T.; Takesue, T. Effect of branching of polyolefin backbone chain on catalytic gasification reaction. *J. Appl. Polym. Sci.* **1989**, *38*, 1491−1501. (b) Lamb, J. V.; Lee, Y.-H.; Sun, J.; Byron, C.; Uppuluri, R.; Kennedy, R. M.; Meng, C.; Behera, R. K.; Wang, Y.-Y.; Qi, L.; Sadow, A. D.; Huang, W.; Ferrandon, M. S.; Scott, S. L.; Poeppelmeier, K. R.; Abu-Omar, M. M.; Delferro, M. Supported Platinum Nanoparticles Catalyzed Carbon−Carbon Bond Cleavage of Polyolefins: Role of the Oxide Support Acidity. *ACS Appl. Mater. Interfaces* **2024**, *16*, 11361−11376.

(7) Cen, Z.; Han, X.; Lin, L.; Yang, S.; Han, W.; Wen, W.; Yuan, W.; Dong, M.; Ma, Z.; Li, F.; Ke, Y.; Dong, J.; Zhang, J.; Liu, S.; Li, J.; Li, Q.; Wu, N.; Xiang, J.; Wu, H.; Cai, L.; Hou, Y.; Cheng, Y.; Daemen, L. L.; Ramirez-Cuesta, A. J.; Ferrer, P.; Grinter, D. C.; Held, G.; Liu, Y.; Han, B. Upcycling of polyethylene to gasoline through a self-supplied hydrogen strategy in a layered self-pillared zeolite. *Nat. Chem.* **2024**, *16*, 871−880.

(8) Coumans, F.; Mezari, B.; Zuidema, N.; Heinrichs, J. M. J. J.; Hensen, E. J. M. Isolating Al Surface Sites in Amorphous Silica−Alumina by Homogeneous Deposition of Al^{3+} on SiO_2 Nanoparticles. *ACS Appl. Nano Mater.* **2024**, *7*, 25524−25534.

(9) Busca, G. Silica-alumina catalytic materials: A critical review. *Catal. Today* **2020**, *357*, 621−629.

(10) (a) Mouat, A. R.; George, C.; Kobayashi, T.; Pruski, M.; van Duyne, R. P.; Marks, T. J.; Stair, P. C. Highly Dispersed SiO_x/Al_2O_3 Catalysts Illuminate the Reactivity of Isolated Silanol Sites. *Angew. Chem., Int. Ed.* **2015**, *54*, 13346−13351. (b) Valla, M.; Stadler, D.; Mougel, V.; Copéret, C. Switching on the Metathesis Activity of Re-Oxo Alkylidene Surface Sites through a Tailor-Made Silica−Alumina Support. *Angew. Chem., Int. Ed.* **2016**, *55*, 1124−1127. (c) Caillot, M.; Chaumonnot, A.; Digne, M.; Poleunis, C.; Debecker, D. P.; van Bokhoven, J. A. Synthesis of amorphous aluminosilicates by grafting: Tuning the building and final structure of the deposit by selecting the appropriate synthesis conditions. *Microporous Mesoporous Mater.* **2014**, *185*, 179−189.

(11) (a) Valla, M.; Rossini, A. J.; Caillot, M.; Chizallet, C.; Raybaud, P.; Digne, M.; Chaumonnot, A.; Lesage, A.; Emsley, L.; van Bokhoven, J. A.; Copéret, C. Atomic Description of the Interface between Silica and Alumina in Aluminosilicates through Dynamic Nuclear Polarization Surface-Enhanced NMR Spectroscopy and First-Principles Calculations. *J. Am. Chem. Soc.* **2015**, *137*, 10710−10719. (b) Hensen, E. J. M.; Poduval, D. G.; Degirmenci, V.; Ligthart, D. A. J. M.; Chen, W.; Maugé, F.; Rigutto, M. S.; Veen, J. A. R. v. Acidity Characterization of Amorphous Silica−Alumina. *J. Phys. Chem. C* **2012**, *116*, 21416−21429. (c) Wang, Z.; Jiang, Y.; Baiker, A.; Hunger, M.; Huang, J. Promoting Aromatic C−H Activation through Reactive Brønsted Acid−Base Pairs on Penta-Coordinated Al-Enriched Amorphous Silica−Alumina. *J. Phys. Chem. Lett.* **2022**, *13*, 486−491.

(12) (a) Culver, D. B.; Venkatesh, A.; Huynh, W.; Rossini, A. J.; Conley, M. P. $Al(OR^F)_3$ (R^F = $C(CF_3)_3$) activated silica: a well-defined weakly coordinating surface anion. *Chem. Sci.* **2020**, *11*, 1510−1517. (b) Samudrala, K. K.; Huynh, W.; Dorn, R. W.; Rossini, A. J.; Conley, M. P. Formation of a Strong Heterogeneous Aluminum Lewis Acid on Silica. *Angew. Chem., Int. Ed.* **2022**, *61*, No. e202205745.

(13) Chen, L.; Wang, Q.; Hu, B.; Lafon, O.; Trébosc, J.; Deng, F.; Amoureux, J.-P. Measurement of hetero-nuclear distances using a symmetry-based pulse sequence in solid-state NMR. *Phys. Chem. Chem. Phys.* **2010**, *12*, 9395−9405.

(14) Cunningham, J.; Perras, F. A. INTERFACES. A program for determining the 3D structures of surfaces sites using NMR data. *J. Magn. Reson. Open* **2022**, *12*−*13*, 100066.

(15) Taoufik, M.; Szeto, K. C.; Merle, N.; Rosal, I. D.; Maron, L.; Trébosc, J.; Tricot, G.; Gauvin, R. M.; Delevoye, L. Heteronuclear NMR Spectroscopy as a Surface-Selective Technique: A Unique Look

at the Hydroxyl Groups of γ-Alumina. *Chem.—Eur. J.* **2014**, *20*, 4038−4046.
(16) (a) Gan, Z. Measuring multiple carbon−nitrogen distances in natural abundant solids using R-RESPDOR NMR. *Chem. Commun.* **2006**, 4712−4714. (b) Nimerovsky, E.; Gupta, R.; Yehl, J.; Li, M.; Polenova, T.; Goldbourt, A. Phase-modulated LA-REDOR: A robust, accurate and efficient solid-state NMR technique for distance measurements between a spin-1/2 and a quadrupole spin. *J. Magn. Reson.* **2014**, *244*, 107−113.
(17) Jammee, R.; Kolganov, A.; Groves, M. C.; Pidko, E. A.; Sydora, O. L.; Conley, M. P. C−H Bond Activation by Sulfated Zirconium Oxide is Mediated by a Sulfur-Centered Lewis Superacid. *Angew. Chem., Int. Ed.* **2025**, *64*, No. e202421699.
(18) Zheng, A.; Liu, S.-B.; Deng, F. ^{31}P NMR Chemical Shifts of Phosphorus Probes as Reliable and Practical Acidity Scales for Solid and Liquid Catalysts. *Chem. Rev.* **2017**, *117*, 12475−12531.
(19) (a) Erdmann, P.; Greb, L. What Distinguishes the Strength and the Effect of a Lewis Acid: Analysis of the Gutmann−Beckett Method. *Angew. Chem., Int. Ed.* **2022**, *61*, No. e202114550. (b) Großekappenberg, H.; Reißmann, M.; Schmidtmann, M.; Müller, T. Quantitative Assessment of the Lewis Acidity of Silylium Ions. *Organometallics* **2015**, *34*, 4952−4958.
(20) Cheng, H. N.; Smith, D. A. Carbon-13 NMR studies of low-molecular-weight ethylene-propylene copolymers and characterization of polymer chain ends. *Macromolecules* **1986**, *19*, 2065−2072.
(21) Zhang, F.; Zeng, M.; Yappert, R. D.; Sun, J.; Lee, Y.-H.; LaPointe, A. M.; Peters, B.; Abu-Omar, M. M.; Scott, S. L. Polyethylene upcycling to long-chain alkylaromatics by tandem hydrogenolysis/aromatization. *Science* **2020**, *370*, 437−441.
(22) Wischert, R.; Copéret, C.; Delbecq, F.; Sautet, P. Optimal Water Coverage on Alumina: A Key to Generate Lewis Acid−Base Pairs that are Reactive Towards the C H Bond Activation of Methane. *Angew. Chem., Int. Ed.* **2011**, *50*, 3202−3205.
(23) Dai, L.; Zhou, N.; Lv, Y.; Cheng, Y.; Wang, Y.; Liu, Y.; Cobb, K.; Chen, P.; Lei, H.; Ruan, R. Pyrolysis technology for plastic waste recycling: A state-of-the-art review. *Prog. Energy Combust. Sci.* **2022**, *93*, 101021.
(24) Poutsma, M. L. Reexamination of the Pyrolysis of Polyethylene: Data Needs, Free-Radical Mechanistic Considerations, and Thermochemical Kinetic Simulation of Initial Product-Forming Pathways. *Macromolecules* **2003**, *36*, 8931−8957.
(25) Dufaud, V.; Basset, J.-M. Catalytic Hydrogenolysis at Low Temperature and Pressure of Polyethylene and Polypropylene to Diesels or Lower Alkanes by a Zirconium Hydride Supported on Silica-Alumina: A Step Toward Polyolefin Degradation by the Microscopic Reverse of Ziegler−Natta Polymerization. *Angew. Chem., Int. Ed.* **1998**, *37*, 806−810.
(26) Mason, A. H.; Motta, A.; Das, A.; Ma, Q.; Bedzyk, M. J.; Kratish, Y.; Marks, T. J. Rapid atom-efficient polyolefin plastics hydrogenolysis mediated by a well-defined single-site electrophilic/cationic organo-zirconium catalyst. *Nat. Commun.* **2022**, *13*, 7187.
(27) (a) Gao, J.; Zhu, L.; Conley, M. P. Cationic Tantalum Hydrides Catalyze Hydrogenolysis and Alkane Metathesis Reactions of Paraffins and Polyethylene. *J. Am. Chem. Soc.* **2023**, *145*, 4964−4968. (b) Gao, J.; Zhu, L.; Conley, M. P. Polypropylene Degradation Catalyzed by Tantalum Hydrides Supported on Sulfated Alumina. *ACS Catal.* **2023**, *13*, 10765−10769. (c) Lai, Q.; Mason, A. H.; Agarwal, A.; Edenfield, W. C.; Zhang, X.; Kobayashi, T.; Kratish, Y.; Marks, T. J. Rapid Polyolefin Hydrogenolysis by a Single-Site Organo-Tantalum Catalyst on a Super-Acidic Support: Structure and Mechanism. *Angew. Chem., Int. Ed.* **2023**, *62*, No. e202312546.
(28) (a) Kanbur, U.; Paterson, A. L.; Rodriguez, J.; Kocen, A. L.; Yappert, R.; Hackler, R. A.; Wang, Y.-Y.; Peters, B.; Delferro, M.; LaPointe, A. M.; Coates, G. W.; Perras, F. A.; Sadow, A. D. Zirconium-Catalyzed C−H Alumination of Polyolefins, Paraffins, and Methane. *J. Am. Chem. Soc.* **2023**, *145*, 2901−2910. (b) Kanbur, U.; Zang, G.; Paterson, A. L.; Chatterjee, P.; Hackler, R. A.; Delferro, M.; Slowing, I. I.; Perras, F. A.; Sun, P.; Sadow, A. D. Catalytic carbon-carbon bond cleavage and carbon-element bond formation give new life for polyolefins as biodegradable surfactants. *Chem* **2021**, *7*, 1347−1362.
(29) (a) Celik, G.; Kennedy, R. M.; Hackler, R. A.; Ferrandon, M.; Tennakoon, A.; Patnaik, S.; LaPointe, A. M.; Ammal, S. C.; Heyden, A.; Perras, F. A.; Pruski, M.; Scott, S. L.; Poeppelmeier, K. R.; Sadow, A. D.; Delferro, M. Upcycling Single-Use Polyethylene into High-Quality Liquid Products. *ACS Cent. Sci.* **2019**, *5*, 1795−1803. (b) Rorrer, J. E.; Beckham, G. T.; Román-Leshkov, Y. Conversion of Polyolefin Waste to Liquid Alkanes with Ru-Based Catalysts under Mild Conditions. *JACS Au* **2021**, *1*, 8−12. (c) Wang, C.; Xie, T.; Kots, P. A.; Vance, B. C.; Yu, K.; Kumar, P.; Fu, J.; Liu, S.; Tsilomelekis, G.; Stach, E. A.; Zheng, W.; Vlachos, D. G. Polyethylene Hydrogenolysis at Mild Conditions over Ruthenium on Tungstated Zirconia. *JACS Au* **2021**, *1*, 1422−1434. (d) Tennakoon, A.; Wu, X.; Paterson, A. L.; Patnaik, S.; Pei, Y.; LaPointe, A. M.; Ammal, S. C.; Hackler, R. A.; Heyden, A.; Slowing, I. I.; Coates, G. W.; Delferro, M.; Peters, B.; Huang, W.; Sadow, A. D.; Perras, F. A. Catalytic upcycling of high-density polyethylene via a processive mechanism. *Nat. Catal.* **2020**, *3*, 893−901. (e) Peczak, I. L.; Kennedy, R. M.; Hackler, R. A.; Lee, B.; Meirow, M.; Luijten, E.; Poeppelmeier, K. R.; Delferro, M. Treasuring trash: Pt/SrTiO3 catalysts process plastic waste into high-value materials. *Matter* **2023**, *6*, 3296−3321.
(30) Chen, S.; Tennakoon, A.; You, K.-E.; Paterson, A. L.; Yappert, R.; Alayoglu, S.; Fang, L.; Wu, X.; Zhao, T. Y.; Lapak, M. P.; Saravanan, M.; Hackler, R. A.; Wang, Y.-Y.; Qi, L.; Delferro, M.; Li, T.; Lee, B.; Peters, B.; Poeppelmeier, K. R.; Ammal, S. C.; Bowers, C. R.; Perras, F. A.; Heyden, A.; Sadow, A. D.; Huang, W. Ultrasmall amorphous zirconia nanoparticles catalyse polyolefin hydrogenolysis. *Nat. Catal.* **2023**, *6*, 161−173.
(31) (a) Conk, R. J.; Hanna, S.; Shi, J. X.; Yang, J.; Ciccia, N. R.; Qi, L.; Bloomer, B. J.; Heuvel, S.; Wills, T.; Su, J.; Bell, A. T.; Hartwig, J. F. Catalytic deconstruction of waste polyethylene with ethylene to form propylene. *Science* **2022**, *377*, 1561−1566. (b) Wang, N. M.; Strong, G.; DaSilva, V.; Gao, L.; Huacuja, R.; Konstantinov, I. A.; Rosen, M. S.; Nett, A. J.; Ewart, S.; Geyer, R.; Scott, S. L.; Guironnet, D. Chemical Recycling of Polyethylene by Tandem Catalytic Conversion to Propylene. *J. Am. Chem. Soc.* **2022**, *144*, 18526−18531. (c) Conk, R. J.; Stahler, J. F.; Shi, J. X.; Yang, J.; Lefton, N. G.; Brunn, J. N.; Bell, A. T.; Hartwig, J. F. Polyolefin waste to light olefins with ethylene and base-metal heterogeneous catalysts. *Science* **2024**, *385*, 1322−1327.
(32) Zhang, W.; Kim, S.; Wahl, L.; Khare, R.; Hale, L.; Hu, J.; Camaioni, D. M.; Gutiérrez, O. Y.; Liu, Y.; Lercher, J. A. Low-temperature upcycling of polyolefins into liquid alkanes via tandem cracking-alkylation. *Science* **2023**, *379*, 807−811.
(33) (a) Sullivan, K. P.; Werner, A. Z.; Ramirez, K. J.; Ellis, L. D.; Bussard, J. R.; Black, B. A.; Brandner, D. G.; Bratti, F.; Buss, B. L.; Dong, X.; Haugen, S. J.; Ingraham, M. A.; Konev, M. O.; Michener, W. E.; Miscall, J.; Pardo, I.; Woodworth, S. P.; Guss, A. M.; Román-Leshkov, Y.; Stahl, S. S.; Beckham, G. T. Mixed plastics waste valorization through tandem chemical oxidation and biological funneling. *Science* **2022**, *378*, 207−211. (b) Rabot, C.; Chen, Y.; Bijlani, S.; Chiang, Y.-M.; Oakley, C. E.; Oakley, B. R.; Williams, T. J.; Wang, C. C. C. Conversion of Polyethylenes into Fungal Secondary Metabolites. *Angew. Chem., Int. Ed.* **2023**, *62*, No. e202214609.
(34) (a) Chupas, P. J.; Grey, C. P. Surface modification of fluorinated aluminas: Application of solid state NMR spectroscopy to the study of acidity and surface structure. *J. Catal.* **2004**, *224*, 69−79. (b) Kemnitz, E.; Menz, D.-H. Fluorinated metal oxides and metal fluorides as heterogeneous catalysts. *Prog. Solid State Chem.* **1998**, *26*, 97−153. (c) Comas-Vives, A.; Schwarzwälder, M.; Copéret, C.; Sautet, P. Carbon−Carbon Bond Formation by Activation of CH_3F on Alumina. *J. Phys. Chem. C* **2015**, *119*, 7156−7163.
(35) (a) Mao, W.; Bai, Y.; Jia, Z.; Qin, Y.; Wang, B.; Zhang, W.; Lu, J.; Kemnitz, E. The ethylene glycol-mediated sol−gel synthesis of nano AlF_3: structural and acidic properties after different post treatments. *Dalton Trans.* **2022**, *51*, 935−945. (b) Kemnitz, E.; Noack, J. The non-aqueous fluorolytic sol−gel synthesis of nanoscaled metal fluorides. *Dalton Trans.* **2015**, *44*, 19411−19431.

https://doi.org/10.1021/jacs.5c04524
J. Am. Chem. Soc. 2025, 147, 18145−18154

(36) (a) Fujdala, K. L.; Brutchey, R. L.; Tilley, T. D. Tailored Oxide Materials via Thermolytic Molecular Precursor (TMP) Methods. In *Surface and Interfacial Organometallic Chemistry and Catalysis*; *Topics in Organometallic Chemistry*; Springer, 2005; pp 69−115. (b) Copéret, C. Single-Sites and Nanoparticles at Tailored Interfaces Prepared via Surface Organometallic Chemistry from Thermolytic Molecular Precursors. *Acc. Chem. Res.* **2019**, *52*, 1697−1708.
(37) (a) Kraft, A.; Trapp, N.; Himmel, D.; Böhrer, H.; Schlüter, P.; Scherer, H.; Krossing, I. Synthesis, Characterization, and Application of Two $Al(OR^F)_3$ Lewis Superacids. *Chem.-Eur. J.* **2012**, *18*, 9371−9380. (b) Müller, L. O.; Himmel, D.; Stauffer, J.; Steinfeld, G.; Slattery, J.; Santiso-Quiñones, G.; Brecht, V.; Krossing, I. Simple Access to the Non-Oxidizing Lewis Superacid $PhF{\rightarrow}Al(OR^F)_3$ (R^F=$C(CF_3)_3$). *Angew. Chem., Int. Ed.* **2008**, *47*, 7659−7663.
(38) (a) Blake, P. G.; Pritchard, H. The thermal decomposition of trifluoroacetic acid. *J. Chem. Soc. B: Physical Organic* **1967**, 282−286. (b) Butler, J. N. The Thermal Decomposition of Octafluorocyclobutane. *J. Am. Chem. Soc.* **1962**, *84*, 1393−1398. (c) Wang, J.; Lin, Z.; He, X.; Song, M.; Westerhoff, P.; Doudrick, K.; Hanigan, D. Critical Review of Thermal Decomposition of Per- and Polyfluoroalkyl Substances: Mechanisms and Implications for Thermal Treatment Processes. *Environ. Sci. Technol.* **2022**, *56*, 5355−5370.
(39) Chizallet, C.; Bouchy, C.; Larmier, K.; Pirngruber, G. Molecular Views on Mechanisms of Brønsted Acid-Catalyzed Reactions in Zeolites. *Chem. Rev.* **2023**, *123*, 6107−6196.
(40) McVicker, G. B.; Kramer, G. M.; Ziemiak, J. J. Conversion of isobutane over solid acids—A sensitive mechanistic probe reaction. *J. Catal.* **1983**, *83*, 286−300.
(41) Fokin, A. A.; Schreiner, P. R. Selective Alkane Transformations via Radicals and Radical Cations: Insights into the Activation Step from Experiment and Theory. *Chem. Rev.* **2002**, *102*, 1551−1594.
(42) Bard, A. J. Inner-Sphere Heterogeneous Electrode Reactions. Electrocatalysis and Photocatalysis: The Challenge. *J. Am. Chem. Soc.* **2010**, *132*, 7559−7567.
(43) Mayer, J. M. Bonds over Electrons: Proton Coupled Electron Transfer at Solid−Solution Interfaces. *J. Am. Chem. Soc.* **2023**, *145*, 7050−7064.
(44) Buekens, A. G.; Froment, G. F. Thermal Cracking of Isobutane. Kinetics and Product Distributions. *Ind. Eng. Chem. Process Des. Dev.* **1971**, *10*, 309−315.

https://doi.org/10.1021/jacs.5c04524
J. Am. Chem. Soc. 2025, 147, 18145−18154